Monthly Notices of the ROYAL ASTRONOMICAL SOCIETY

MNRAS **525,** 5033–5040 (2023) https://doi.org/10.1093/mnras/stad2598
Advance Access publication 2023 August 31

Comparison of damping models for kink oscillations of coronal loops

Yu Zhong,[1] Dmitrii Y. Kolotkov [1,2] Sihui Zhong [1] and Valery M. Nakariakov [1,3]★

[1]*Centre for Fusion, Space and Astrophysics, Department of Physics, University of Warwick, Coventry CV4 7AL, UK*
[2]*Engineering Research Institute 'Ventspils International Radio Astronomy Centre (VIRAC)', Ventspils University of Applied Sciences, LV-3601 Ventspils, Latvia*
[3]*Centro de Investigacion en Astronomía, Universidad Bernardo O'Higgins, Avenida Viel 1497, Santiago 8370993, Chile*

Accepted 2023 August 21. in original form 2023 July 31

ABSTRACT

Kink oscillations of solar coronal loops are of intense interest due to their potential for diagnosing plasma parameters in the corona. The accurate measurement of the kink oscillation damping time is crucial for precise seismological diagnostics, such as the transverse density profile, and for the determination of the damping mechanism. Previous studies of large-amplitude rapidly decaying kink oscillations have shown that both an exponential damping model and a generalized model (consisting of Gaussian and exponential damping patterns) fit observed damping profiles sufficiently well. However, it has recently been shown theoretically that the transition from the decaying regime to the decayless regime could be characterized by a superexponential damping model. In this work, we reanalyse a sample of decaying kink oscillation events, and utilize the Markov chain Monte Carlo Bayesian approach to compare the exponential, Gaussian–exponential, and superexponential damping models. It is found that in 7 out of 10 analysed oscillations, the preferential damping model is the superexponential one. In two events, the preferential damping is exponential, and in one it is Gaussian–exponential. This finding indicates the plausibility of the superexponential damping model. The possibility of a non-exponential damping pattern needs to be taken into account in the analysis of a larger number of events, especially in the estimation of the damping time and its associated empirical scalings with the oscillation period and amplitude, and in seismological inversions.

Key words: waves – Sun: corona – Sun: oscillations.

1 INTRODUCTION

Kink oscillations of plasma loops that form active regions of the corona are among the most studied wave phenomena in the solar atmosphere (e.g. Nakariakov & Kolotkov 2020; Nakariakov et al. 2021). The oscillations are usually seen as oscillatory transverse displacements of bright loops in the plane of the sky with high-resolution extreme ultraviolet (EUV) imagers, such as the Transition Region and Coronal Explorer (TRACE), Solar Dynamics Observatory/Atmospheric Imaging Assembly (SDO/AIA), and the Solar Orbiter Extreme Ultraviolet Imager (SolO/EUI) (e.g. Aschwanden et al. 1999, 2002; Nakariakov et al. 1999; Aschwanden & Schrijver 2011; Zhong et al. 2022), respectively. Kink oscillations have also been found as periodic Doppler shifts of coronal emission lines, i.e. as periodic movements of the emitting plasma along the line of sight (Tian et al. 2012). Kink oscillations attract attention as a highly useful tool for probing physical parameters of coronal active regions, such as the absolute value of the magnetic field (e.g. Nakariakov & Ofman 2001), density stratification, and the dependence of the magnetic field on height (e.g. Andries, Arregui & Goossens 2005; Ruderman, Verth & Erdélyi 2008), as well as in the context of heating of the solar corona (see e.g. Van Doorsselaere et al. 2020, for a recent comprehensive review).

Kink oscillations appear in two distinct regimes, the large-amplitude rapidly decaying oscillations (e.g. Nakariakov et al. 1999; Goddard et al. 2016; Nechaeva et al. 2019) and low-amplitude decayless oscillations (e.g. Wang et al. 2012; Anfinogentov, Nisticò & Nakariakov 2013). In both regimes, the oscillation is a standing wave, with the nodes at the footpoints. In the majority of cases, kink oscillations have maximum displacement amplitudes near the loop top, i.e. correspond to the fundamental harmonic, while higher harmonics have been detected too (e.g. De Moortel & Brady 2007; Andries et al. 2009). Typical oscillation periods are several minutes. The periods are observed to increase with the increase in the loop length (Anfinogentov et al. 2013; Nechaeva et al. 2019). The phase speed is estimated by the ratio of the wavelength and the oscillation period. In the majority of cases, decaying oscillations are excited by a displacement of the loop from an equilibrium by a low coronal eruption (Zimovets & Nakariakov 2015). Typical initial displacement amplitudes of decaying kink oscillations are several megametres. In the decayless regime, oscillation amplitudes are much lower, typically smaller than a few hundred kilometres. Nisticò, Nakariakov & Verwichte (2013) observed an oscillatory decay of a displaced loop to a stationary, i.e. decayless, oscillation.

There is a wealth of theoretical studies interpreting the damping of kink oscillations as linear transformation of a collective mode into highly localized torsional Alfvénic oscillations of individual surfaces of a constant Alfvén speed (e.g. Goossens, Hollweg & Sakurai 1992; Ruderman & Roberts 2002; Goossens, Andries & Arregui 2006). According to the theory, in the initial stage of the kink oscillation, the amplitude decreases as a Gaussian function, followed by an exponential decay (e.g. Pascoe et al. 2013). The Gaussian decay

★ E-mail: V.Nakariakov@warwick.ac.uk

phase is pronounced in loops with low contrasts of external and internal densities. Such a combined, Gaussian–exponential damping pattern has been observationally confirmed by Pascoe et al. (2016a,b, 2017) and Pascoe, Goddard & Van Doorsselaere (2020). However, in the analysis of kink oscillation, the Gaussian decay phase is often neglected, and, in particular, the damping time is estimated by an exponentially decaying oscillation envelope (see e.g. Ofman & Aschwanden 2002; Goddard et al. 2016; Nechaeva et al. 2019; Dai et al. 2021; Mandal, Tian & Peter 2021; Conde, Jain & Jatenco-Pereira 2022; Zhang et al. 2022, for some more recent works). Other damping mechanisms may be wave tunnelling or leakage, caused by the active region geometry and other 3D effects (e.g. Brady, Verwichte & Arber 2006; Selwa, Ofman & Solanki 2011; Hindman & Jain 2014). Moreover, there is a growing theoretical evidence that the decay may actually be a non-linear process such as Kelvin–Helmholtz instability (KHI; e.g. Terradas et al. 2008; Magyar & Van Doorsselaere 2016; Van Doorsselaere et al. 2021; Ruderman & Petrukhin 2022). The non-linear nature of the damping is also indicated by the empirically established dependence of the oscillation quality factor, i.e. the ratio of the damping time to the oscillation period upon the amplitude (Goddard & Nakariakov 2016; Nechaeva et al. 2019; Arregui 2021). A non-linear decay pattern is not necessarily an exponential one. For example, the low-dimensional modelling of the decay of an impulsively excited kink oscillation to the stationary oscillation driven by a self-oscillatory mechanism demonstrated its superexponential nature (Nakariakov & Yelagandula 2023). Thus, the choice of the model function for empirical fitting decay patterns of kink oscillations remains an open question.

The aim of this paper is to compare the exponential, superexponential, and Gaussian–exponential models, applying them to several randomly selected kink oscillation events. An additional aim is to validate the need for accounting for the superexponential damping regime, and the associated re-evaluation of the damping times. We do this on a small sample of events, before performing a very laborious reanalysis of all 223 oscillations in the catalogue of Nechaeva et al. (2019). The comparison is performed by assessing the mutual Bayesian factors of the chosen damping models (e.g. Arregui 2018, 2022; Anfinogentov et al. 2022). In Section 2, we demonstrate the data and analytical technique used in this study. In Section 3, we compare oscillation damping with three theoretical models using observed signals. A summary of the findings and discussions are presented in Section 4.

2 OBSERVATIONAL DATA ANALYSIS

In the previous work, Nechaeva et al. (2019) created a comprehensive catalogue of decaying kink oscillations of 223 solar coronal loops, extending from the works of Zimovets & Nakariakov (2015) and Goddard et al. (2016). The catalogue provides general information about each loop, including slit position, starting time of oscillation, oscillation period and amplitude, exponential damping time, and other physical parameters. For our analysis, we select two events that have been previously studied by Nisticò et al. (2013) and Pascoe et al. (2016a,b, 2017) for comparison, and eight other randomly selected events from the catalogue of Nechaeva et al. (2019).

A summary of the key physical parameters of the selected oscillation events and host loops is given in Table 1. As seen in this table, all of the oscillating loops are situated off the solar limb. Nine events are associated with solar flares. For loops L1 and L2, the estimations of the loop lengths and oscillation amplitudes are given without the error bars, as it is in the catalogue of Nechaeva et al. (2019).

We use EUV image sequences of the host solar coronal active regions, taken with the AIA (Lemen et al. 2012) onboard SDO (Pesnell, Thompson & Chamberlin 2012) to investigate the damping properties of our kink oscillation events. For each event, 900 image frames at the 171 Å channel with a spatial resolution of 0.6 arcsec and a time cadence of 12 s are requested from the Joint Science Operations Center. We cut out image sequences after performing the differential rotation correction on the processed level 1.5 data.

The regions of interest are 250 pixels × 250 pixels in size, centred by the slit mid-points (see Table 1). The time duration of each data set is 3 h, covering the full oscillation of each loop.

Then, time–distance (TD) analysis is performed to obtain the oscillation signals. To create TD maps, we take linear slits perpendicular to the oscillating loop in the vicinity of the loop apex, whose positions are provided by Nechaeva et al. (2019). For each event, slits are 5 pixels in width, and the average value of intensity over this width is calculated to increase the signal-to-noise ratio.

The decaying oscillating perpendicular displacements are clearly observed by eye in the TD maps for the considered oscillating loops (see Figs 1 and A1).

2.1 Loop-tracking algorithms

A time series of oscillating displacements of a loop is obtained from TD map by an automated loop-tracking technique. At each instant of time in the TD map, we extract the loop's intensity profile along the slit (see Fig. 2), and estimate the location of the loop centre or one of its boundaries mainly by fitting with a prescribed function.

In this study, the following six tracking algorithms (depicted in Fig. 2) are adopted to obtain the oscillatory displacements of loop centres or boundaries:

(i) A Gaussian function is applied to fit the loop's intensity profile, resulting in a time series for the position of the peak brightness across the oscillating loop [Fig. 2(a)]. Since the full width at half-maximum (FWHM) is usually taken as the characteristic loop width (e.g Wang et al. 2012; Klimchuk & DeForest 2020) in observations, we set this quantity as the fitting range for the following algorithms (ii)–(iv).

(ii) A parabolic function is applied to fit the intensity profile within the FWHM estimated at step (i), thereby determining the position of the peak brightness by its local maximum [Fig. 2(b)].

(iii) Similar to (ii) but with a cubic parabolic function [Fig. 2(c)].

(iv) An area integral under the intensity curve is calculated, and positions of the area bisector lines are taken as loop centre positions [Fig. 2(d)].

(v) A Gaussian function is applied to fit the spatial derivatives (Anfinogentov et al. 2013) of intensity profile across one-half of the loop. The Gaussian fitting centre indicates the highest (negative) gradient of the loop's intensity profile, i.e. the loop boundary [Fig. 2(e)].

(vi) A hyperbolic tangent function, $F(x) = A \tanh\left(\frac{x-x_0}{\Delta}\right) + C$, where A, Δ, and C are arbitrary constants determined by the fitting procedure, is applied to fit intensity profiles across one-half of the loop. The inflexion point given by x_0 is used to indicate the position of the loop boundary [Fig. 2(f)]. Fitting is performed with the routine `mpfit.pro` in IDL.

The dependence of the oscillation properties on the loop-tracking algorithms is of interest. We take oscillating loops L5, L6, L10, and L2 (see Fig. 1) as an example to demonstrate the application of the loop-tracking algorithms described earlier. For each event, we obtain

Table 1. Kink oscillation events under study, randomly selected from the catalogue (Nechaeva et al. 2019). The loop and oscillation parameters are taken from the catalogue. The dash means that the event is not associated with a flare.

No.	Slit mid-point (x, y) (arcsec)	Date	Time (UT)	Flare	Length (Mm)	Period (min)	Osc. amp. (Mm)
L1[a]	954.5, 307	2012 May 26	20:36:47	SOL2012-05-26T20:09	162	7.67 ± 0.04	9.4
L2[a]	−980.5, 354	2012 May 30	08:58:57	SOL2012-05-30T08:35	234	4.28 ± 0.02	8.8
L3	1098, 347	2014 Jul 11	23:40:11	SOL2014-07-11T23:38	489 ± 10	11.83 ± 0.38	7.5 ± 1.3
L4	−1010.5, −14.5	2014 Nov 15	12:00:00	SOL2014-11-15T11:47	200 ± 10	9.27 ± 0.13	7.2 ± 0.8
L5	1151.5, 50	2015 Apr 23	16:55:49	SOL2015-04-23T16:38	431 ± 8	20.43 ± 0.47	14.5 ± 2.6
L6	1128.5, −89.5	2015 Oct 02	03:08:58	–	394 ± 20	17.19 ± 0.76	12.8 ± 3.6
L7	1062.5, 304.5	2015 Oct 27	14:42:10	SOL2015-10-27T13:12	328 ± 10	12.81 ± 0.32	6.1 ± 1.3
L8	−1150.5, −90.5	2015 Dec 20	01:11:58	SOL2015-12-20T01:09	436 ± 9	18.59 ± 0.78	13.4 ± 2.1
L9	−1066.5, 388	2016 Jul 10	00:56:46	SOL2016-07-10T00:50	547 ± 11	10.76 ± 0.28	12.1 ± 1.1
L10	949, −306.5	2017 Sep 07	18:08:45	SOL2017-09-07T18:02	326 ± 9	8.32 ± 0.10	21.5 ± 2.4

[a]Events L1 and L2 are selected from Nisticò et al. (2013) and Pascoe et al. (2016a,b, 2017).

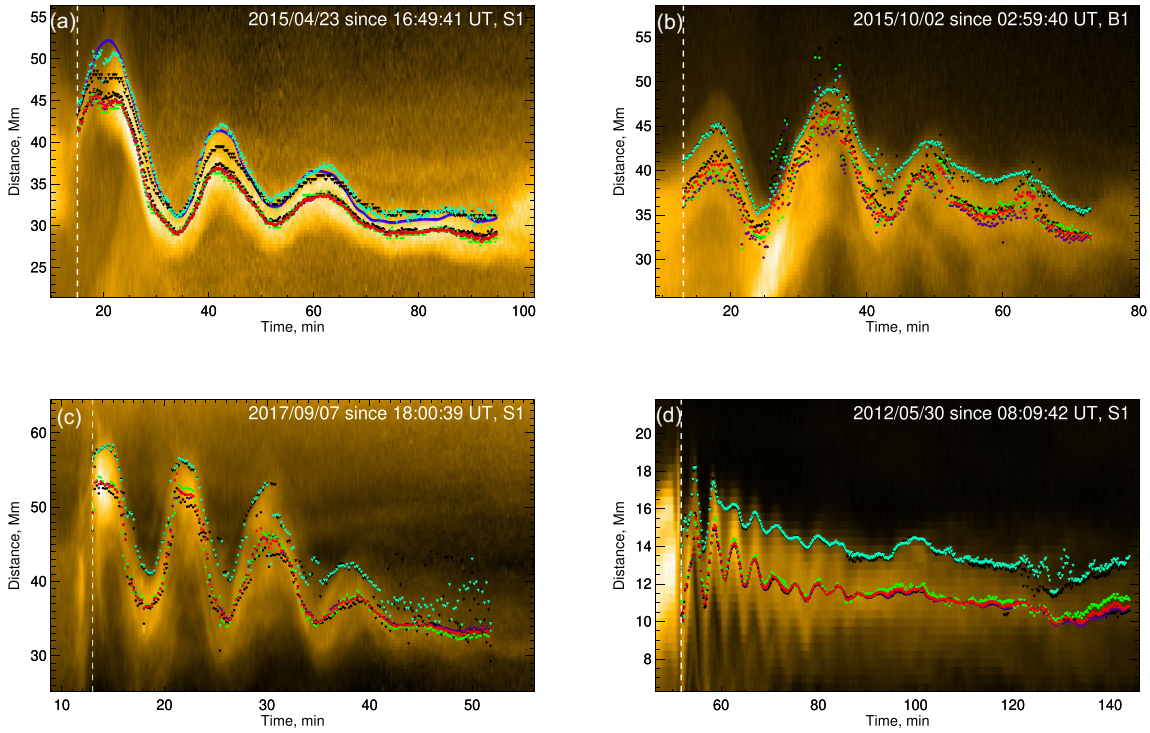

Figure 1. Four typical TD maps with decaying oscillating displacement signals, corresponding to loops L5 (a), L6 (b), L10 (c), and L2 (d). The white vertical dashed lines indicate the start time of oscillations. The black, purple, green, and red dots mark the centre of the oscillating loop by algorithms (i)–(iv), and the black and cyan triangles mark the edge by algorithms (v) and (vi). In panel (a), the blue triangles on the edge of loops indicate the signal determined by eye.

a set of six decaying oscillatory signals with these algorithms, each denoted as $\xi_n(t)$, where n ranges from 1 to 6, respectively. In addition, we add the boundary displacement signal obtained manually, by clicking the TD maps with a cursor, as $\xi_7(t)$, for comparison.

We first manually clicked data points on the upper loop boundary and performed cubic spline interpolation to achieve ξ_7 instantaneous positions in each time frame [see the blue triangles in Fig. 1(a)]. Then, we employed the six automated loop-tracking algorithms (i)–(vi) to compute oscillation signals ξ_1–ξ_6, which are shown in Fig. 1(a) by different coloured symbols.

For L5, the four series of signals ξ_1–ξ_4 tracking the loop centres are situated close to each other and almost indistinguishable. Likewise, the signals ξ_5–ξ_7 outline the outermost oscillating loop boundary well. Among them, signals ξ_5 and ξ_6 appear to be smoother and more rounded compared to ξ_7. L5 has an appropriate width and stands up against the background clearly without overlapping structures. That is why the oscillation signals obtained by different algorithms show good stability, consistency, smoothness, clarity, and data integrity. For other loops, a user should choose an algorithm that works best in each particular case. For example, in Fig. 1(b) the centre signals are contaminated by the overlapped loop structures, so that the boundary-based algorithms (v) and (vi) are better choices. In Fig. 1(c), the loop brightness significantly decreases near the end of the oscillation. The decrease in the loop contrast with the background leads to a more frequent appearance of outliers in the considered loop-tracking algorithms. Also, some interference between oscillation peaks may

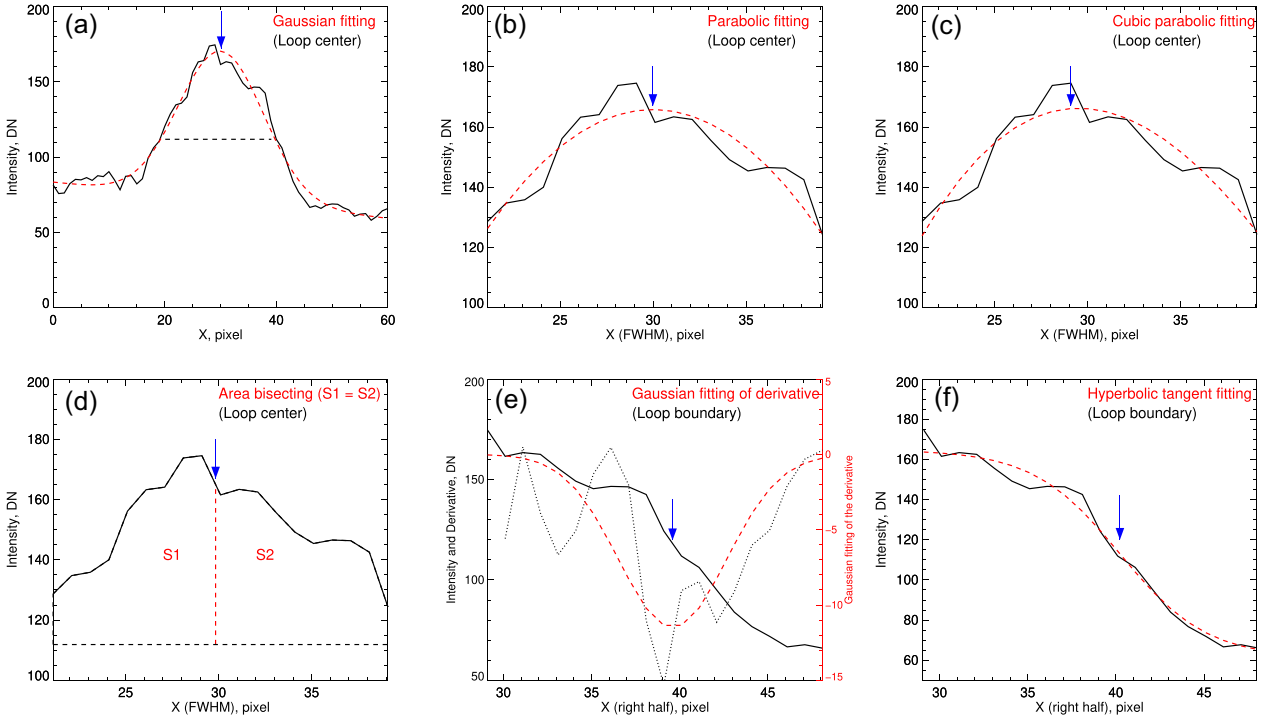

Figure 2. Six algorithms (i)–(vi) to track the loop oscillation signals, respectively. Blue arrows in panels (a)–(d) show the loop centre positions to track ξ_1–ξ_4, and those in panels (e) and (f) show boundary positions in ξ_5 and ξ_6. The red dashed lines represent the fitting results in all panels, except in panel (d), where it represents a bisecting line. The black dotted line in panel (e) represents the derivative of the intensity profile. Intensity profiles are taken from loop L5 as an example.

occur if the oscillation period is too short. Hence, the centre signals are slightly better than the boundary ones in Fig. 1(d). Addressing these results, various extreme situations with low signal to noise, loop contrast, etc., have been comprehensively tested on synthetic data, making sure our methodology is reliable for the following analysis.

2.2 Analysis of oscillation parameters with MCMC Bayesian inference

In order to analyse the oscillatory loop displacements $\xi_n(t)$ derived in Section 2.1 and obtain their parameters, we fit each of them by a decaying harmonic function with a cubic–parabolic background trend,

$$\xi_n(t) = AM(t)\sin\left(\frac{2\pi}{P}t+\varphi\right)+T(t),$$
$$T(t) = a_0 + a_1 t + a_2 t^2 + a_3 t^3, \tag{1}$$

where A is the initial displacement amplitude, $M(t)$ is the oscillation damping model, P is the oscillation period, and φ is the initial phase. The parameters a_0, a_1, a_2, and a_3 are constant coefficients.

In this work, we consider three possible scenarios for the damping of kink oscillations, proposed hitherto. Namely, these three models include exponential damping $M_e(t)$ (e.g. Goossens et al. 1992, 2006; Ruderman & Roberts 2002), Gaussian–exponential damping $M_g(t)$ (Pascoe et al. 2013, 2016a), and superexponential damping $M_s(t)$ (De Moortel, Hood & Ireland 2002; Nakariakov & Yelagandula 2023),

$$M_e(t) = \exp\left(-\frac{t}{\tau_e}\right), \tag{2}$$

$$M_g(t) = \begin{cases} \exp\left(-\dfrac{t^2}{2\tau_g^2}\right), & t \le t_s, \\ A_s \exp\left(-\dfrac{t-t_s}{\tau_{g,e}}\right), & t > t_s, \end{cases} \tag{3}$$

$$M_s(t) = \exp\left[-\left(\frac{t}{\tau_s}\right)^d\right], \tag{4}$$

where τ_e stands for the exponential damping time, τ_g and $\tau_{g,e}$ are the characteristic damping times of the Gaussian and exponential phases in the Gaussian–exponential model, respectively, t_s is the switch time between these two phases, τ_s is the damping time in the superexponential model, and d is the superexponential power index. We set $A_s = \exp(-t_s^2/2\tau_g^2)$ to fulfill the continuity around t_s for the piecewise function given by equation (3). Note that these three damping models have different numbers of free parameters, which is important for their comparison.

We fit the trend $T(t)$ using the `polyfit.pro`. Detrended signals are best fitted with the expressions given by equation (1) with decay models [equations (2)–(4)] with the Solar Bayesian Analysis Toolkit (SOBAT; Anfinogentov et al. 2021) implementing the Bayesian inference with the Markov chain Monte Carlo (MCMC) sampling method. Best-fitting examples for the signals obtained by algorithm (iv) or (vi), described in Section 2.1, are shown in Fig. A1. The green, red, and blue fitting curves stand for the exponential, superexponential, and Gaussian–exponential damping model results, respectively. All ten kink oscillation events are well identified,

Table 2. Bayesian factors, damping times, and physical parameters for the most probable decay model. Parameters M_e, M_s, and M_g stand for exponential, superexponential, and Gaussian–exponential model, respectively. The period and oscillation amplitude values are taken from the preferred model for each event.

No.	$2\ln B_{s,e}$	$2\ln B_{s,g}$	$2\ln B_{e,g}$	Gaussian–exp. $\tau_g/\tau_{g,e}$	Exp. τ_e	Superexp. τ_s	Preferred model	M_s Index d	Period (min)	Osc. amp. (Mm)
L1	2.13	4.23	2.10	$14.75^{+6.33}_{-3.84}/16.85^{+10.84}_{-4.30}$	$21.98^{+9.79}_{-5.04}$	$23.59^{+7.20}_{-2.72}$	M_s	$1.72^{+0.37}_{-0.62}$	$7.75^{+0.19}_{-0.16}$	$8.46^{+1.60}_{-1.80}$
L2	−0.68	2.19	2.07	$13.48^{+0.65}_{-5.86}/11.03^{+4.44}_{-0.71}$	$13.61^{+3.43}_{-2.61}$	$15.77^{+0.69}_{-6.86}$	M_e	$1.18^{+0.42}_{-0.14}$	$4.18^{+0.28}_{-0.07}$	$8.06^{+5.71}_{-0.02}$
L3	28.40	4.75	−23.65	$27.94^{+3.55}_{-3.48}/9.51^{+18.66}_{-7.63}$	$38.76^{+8.64}_{-6.43}$	$40.04^{+3.88}_{-3.66}$	M_s	$2.91^{+2.15}_{-0.82}$	$11.56^{+0.14}_{-0.13}$	$7.47^{+0.74}_{-0.82}$
L4	−3.75	−1.91	1.84	$22.88^{+12.31}_{-9.53}/28.46^{+22.04}_{-16.46}$	$40.36^{+12.77}_{-7.79}$	$39.59^{+16.31}_{-10.28}$	M_e	$1.21^{+0.54}_{-0.26}$	$8.71^{+0.09}_{-0.09}$	$7.95^{+0.96}_{-1.03}$
L5	75.69	14.96	−61.01	$30.13^{+2.07}_{-1.80}/10.03^{+7.44}_{-1.85}$	$34.29^{+3.75}_{-3.34}$	$44.09^{+2.70}_{-2.76}$	M_s	$2.60^{+0.43}_{-0.37}$	$20.42^{+0.26}_{-0.23}$	$11.15^{+0.74}_{-0.71}$
L6	27.97	−6.71	−34.68	$29.52^{+5.00}_{-3.23}/12.43^{+14.14}_{-9.90}$	$50.01^{+21.12}_{-11.10}$	$41.61^{+7.23}_{-4.58}$	M_g	$2.00^{+0.07}_{-0.25}$	$17.03^{+0.56}_{-0.47}$	$9.91^{+0.93}_{-1.22}$
L7	15.80	5.13	−10.67	$25.63^{+5.17}_{-4.85}/13.23^{+18.66}_{-9.60}$	$37.05^{+14.68}_{-8.12}$	$36.86^{+6.21}_{-5.43}$	M_s	$2.48^{+0.47}_{-0.76}$	$11.90^{+0.25}_{-0.27}$	$5.18^{+0.75}_{-0.61}$
L8	123.02	26.35	−96.67	$25.90^{+2.78}_{-2.76}/20.85^{+7.09}_{-3.04}$	$34.78^{+3.10}_{-4.73}$	$38.89^{+4.43}_{-3.64}$	M_s	$2.14^{+0.18}_{-0.27}$	$17.23^{+0.21}_{-0.19}$	$8.70^{+0.66}_{-0.44}$
L9	75.01	15.53	−59.47	$26.76^{+2.61}_{-2.06}/6.72^{+10.58}_{-4.39}$	$33.42^{+6.94}_{-4.76}$	$38.35^{+3.17}_{-2.60}$	M_s	$2.50^{+0.09}_{-0.22}$	$13.14^{+0.20}_{-0.19}$	$8.16^{+0.64}_{-0.67}$
L10	70.76	20.05	−50.71	$15.78^{+2.23}_{-3.13}/5.57^{+8.26}_{-3.32}$	$20.71^{+6.81}_{-3.54}$	$22.88^{+2.72}_{-2.32}$	M_s	$2.72^{+0.08}_{-0.50}$	$8.17^{+0.17}_{-0.15}$	$16.39^{+1.68}_{-1.54}$

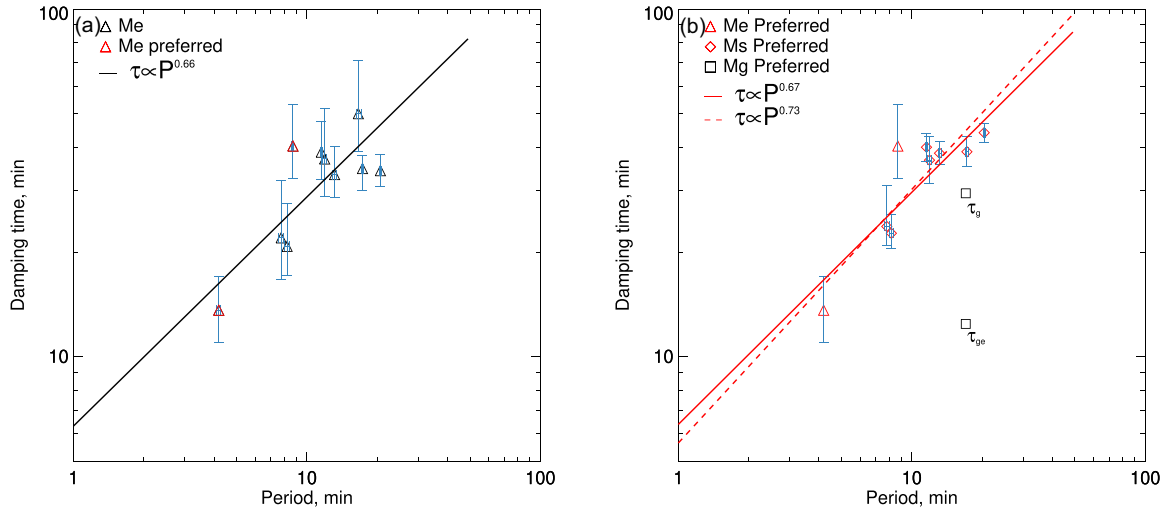

Figure 3. Damping times τ estimated by different models against oscillation periods P in log–log plots. (a): Power-law fit to parameters of 10 loops in exponential model. (b): Power-law fit to preferred parameters of 9 loops (dashed line) and 7 superexponential loops (solid line), respectively. Gradients of the power-law fitting lines in panels (a) and (b), standing for the power-law index, are 0.66 ± 0.17, 0.67 ± 0.16, and 0.73 ± 0.15, respectively. Blue bars indicate the 95 per cent credible intervals of periods and damping times calculated with MCMC method. Two damping times derived from the Gaussian–exponential model are plotted but not included in the fitting process.

tracked, and fitted for more than four consecutive oscillation cycles. The best-fitting oscillation parameters obtained with this fitting procedure are summarized in Table 2.

3 RESULTS OF DAMPING MODEL COMPARISON

In addition to the reliable estimation of the model parameters and their credible intervals, the use of SOBAT enables us to quantitatively compare our three different damping models given by equations (2)–(4) in the application to our 10 kink oscillation events, using the Bayesian factor $B_{i,j}$, which is the ratio of Bayesian evidence of model i to that of model j. The higher value of the Bayesian factor $B_{i,j}$, in general, indicates the preference of model i over model j (see section 5.2 in Anfinogentov et al. 2021, for details).

3.1 Quantitative comparison for observed events

Using `mcmcfit.pro` routine from SOBAT package with 10^6 samples and loop L5 as an example, signals ξ_1–ξ_6 are independently best fitted with three damping models given by equations (2)–(4). Bayesian factors are calculated using `mcmcfitevidence.pro` routine. For ξ_1–ξ_6, the mean values of their Bayesian factors $B_{s,e}$, $B_{s,g}$, and $B_{g,e}$ are 75.69, 14.69, and –61.01 (see Table 2), respectively, averaged over the six automated loop-tracking algorithms. As a validation, the Bayesian factors of ξ_7 show similar values (42.12, 13.47, and −28.65). Thus, we obtain strong evidence in favour of the superexponential model in comparison to the other two models for loop L5. Following this approach, the preferred damping model is identified for each kink oscillation event considered (see Table 2). Namely, the superexponential model has stronger evidence in 7 out of all 10 kink oscillation events, exponential damping is preferred in 2 events, and Gaussian–exponential is preferred in 1 event. For each event, the model parameters (i.e. the oscillation period and projected amplitude, and damping time, and the superexponential power index for the events that are better fitted by that model) are shown for the preferred damping model, averaged over all loop-tracking methods applied in this study.

The obtained oscillation periods and amplitudes are consistent with those from the catalogue of Nechaeva et al. (2019), shown in Table 1, while the oscillation damping time depends upon the choice of the damping model and may differ significantly from its exponential value. We also note that the obtained values of the superexponential power index d are generally consistent with the value of about 2 observed by De Moortel et al. (2002).

3.2 Correlation between the oscillation parameters

According to the analysis presented earlier, we obtain that more than a half of the analysed events exhibit a preference of the superexponential model. As revealed in Table 2, the damping time calculated in the superexponential model is generally greater than that in the exponential model, which in turn is greater than that in the Gaussian–exponential model.

As our analysis demonstrated the sensitivity of the damping time estimation to the chosen damping model, we investigate the dependence of the damping time on the oscillation period, and the association between the quality factor of the oscillations and their amplitude. Fig. 3 shows the scatter diagram of the oscillation damping times versus the corresponding oscillation periods. The 95 per cent credible intervals of the damping time are indicated by the blue error bars in the figure. Previous estimations (Aschwanden et al. 2002; Verwichte et al. 2013; Goddard et al. 2016; Nechaeva et al. 2019) have demonstrated an empirical linear scaling of the damping time with the oscillation period, which is mainly consistent with our results.

To estimate the scaling of the damping time determined by a specific model, with the oscillation period, we use the `linfit.pro` to fit a power-law function to parameter pairs in a logarithmic scale. The fitting of 10 points estimated by the exponential damping model in Fig. 3(a) demonstrates a power-law index of 0.66 ± 0.17. This value is roughly consistent with the result obtained by Nechaeva et al. (2019) under the assumption of the exponential damping. As the damping time in the Gaussian–exponential model is not a single value and this model has the highest preference in only one event in our data set, we exclude that event from estimation. In Fig. 3(b), the parameters $\tau_{\rm g}$ and $\tau_{\rm g,e}$ from the Gaussian–exponential model are shown but not included in any fitting process. As demonstrated by Fig. 3(b), the power-law fits to the preferred model parameters for nine (with preferences in favour of the exponential and superexponential damping models) and seven (the superexponential damping model only) cases are similar, with values of 0.73 ± 0.15 and 0.67 ± 0.16, respectively. The exponential damping time $\tau_{\rm g,e}$ of the Gaussian–exponential model, which is preferred for loop L6 shown in Fig. 3(b) (see the black squares), clearly stands out as an outlier from the best-fitting lines.

Goddard & Nakariakov (2016) and Nechaeva et al. (2019) found that the quality factor Q defined as the ratio of the damping time to the oscillation period depends on the oscillation displacement amplitude, with the dependence approximated by a power law. In those studies, the quality factor was estimated by the exponential damping model. Scaling of Q estimated in our study with the oscillation amplitude is shown in Fig. 4. Only the events that show the preference of the exponential and superexponential damping models are shown. The red dashed curve is the scaling result from Nechaeva et al. (2019). We see that the quality factor Q decreases with the oscillation amplitude, as it has been found before. We need to stress that the fitting curve is determined by the upper outer boundary of the data cloud because of the projection effect (Goddard & Nakariakov 2016; Nechaeva et al. 2019).

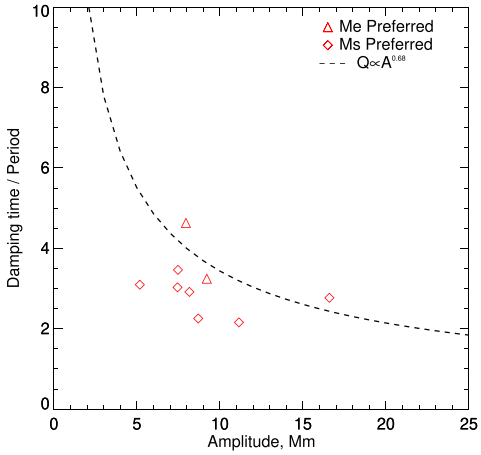

Figure 4. Quality factor Q defined as the ratio of the damping time $t_{\rm e}$ to the oscillation period P in preferred models, plotted against their projected oscillation amplitude. The black dashed line shows the power-law scaling with the index of 0.68, determined in Nechaeva et al. (2019). The symbols in this figure have same meaning as in Fig. 3, including 2 exponential and 7 superexponential data points.

4 DISCUSSION AND CONCLUSIONS

Using the Bayesian analysis method, we performed a comparison of three previously proposed models of damping of kink oscillations in 10 randomly chosen coronal loops. In each event, we extracted oscillatory patterns from a TD map by six different loop-tracking algorithms based on the identification of the instantaneous location of the centre or boundary of the oscillating loop. We demonstrated that those six different algorithms produce rather similar outcomes that do not affect the results. It is found that out of 10 kink oscillations selected for investigation, a superexponential damping model is preferred in 7. In two events, the damping is more aptly described by an exponential model. In one event, the preferential damping model is Gaussian–exponential. This finding indicates that the superexponential decay pattern that was recently proposed theoretically for kink oscillations of a self-oscillatory nature (Nakariakov & Yelagandula 2023) is a plausible model. This result, based on the analysis of a limited number of events, justifies the need for a much more laborious analysis of a larger number of kink oscillation events in a similar fashion.

According to Nakariakov & Yelagandula (2023), the superexponential damping has been found to occur when an impulsively excited oscillation decays not to a zero amplitude, i.e. to an equilibrium, but to a stationary amplitude of a decayless regime. In the data analysis, the stationary amplitude may be lower than observational resolution, and hence the oscillation apparently decays to zero. As an exponential model is a limiting case of the superexponential model, corresponding to the index $d = 1$, the exponential model may still be sufficiently correct in general. Also, our analysis shows that the Gaussian–exponential model performs well in most cases, but a large number of free parameters decreased its advantage in the Bayesian comparison. In all 10 analysed events, longer oscillation periods are found to correspond to longer damping times. Upon further analysis, this relationship generally confirmed a power-law scaling with a consistent exponent of around 0.6–0.7, established in Nechaeva et al. (2019).

The damping model that attributes the kink oscillation damping to the transition to a stationary oscillation in the decayless regime requires further development, including its confirmation by full

magnetohydrodynamic numerical simulations. In particular, it should be investigated whether the superexponential function is indeed the best analytical expression for that process. Other open questions are whether the index d is actually significantly different from unity and whether there is a combined Gaussian–superexponential decay pattern.

The small number of the analysed events, only 10, does not allow us to make rigorous conclusions about the empirical occurrence rates of various damping regimes. However, our findings indicate the need for reconsideration of the events presented in the catalogue of Nechaeva et al. (2019), possibly supplemented by more recent events. The aim of this reconsideration is to determine the preferential damping model for each event, choosing from the exponential, Gaussian–exponential, and superexponential ones, and, possibly, other models provided by theory. For most preferential models, the corresponding damping times should be estimated. Analysis of empirical scalings of various oscillation parameters requires the use of corrected values of the damping times and quality factors. On the other hand, theoretical modelling of decaying kink oscillations should provide us with scalings typical for various damping mechanisms, including KHI and wave tunnelling and leakage.

ACKNOWLEDGEMENTS

The data used are courtesy of the SDO/AIA team. We gratefully acknowledge advice from Dr D. J. Pascoe and Dr S. A. Anfinogentov. DYK and VMN acknowledge support from the Latvian Council of Science Project No. lzp2022/1-0017. DYK acknowledges support from the STFC consolidated grant ST/X000915/1.

DATA AVAILABILITY

Data we analysed in this paper are from SDO/AIA and available at http://jsoc.stanford.edu/. SOBAT (Anfinogentov et al. 2021) is available at https://github.com/Sergey-Anfinogentov/SoBAT/.

REFERENCES

Andries J., Arregui I., Goossens M., 2005, ApJ, 624, L57
Andries J., van Doorsselaere T., Roberts B., Verth G., Verwichte E., Erdélyi R., 2009, Space Sci. Rev., 149, 3
Anfinogentov S., Nisticò G., Nakariakov V. M., 2013, A&A, 560, A107
Anfinogentov S. A., Nakariakov V. M., Pascoe D. J., Goddard C. R., 2021, ApJS, 252, 11
Anfinogentov S. A. et al., 2022, Space Sci. Rev., 218, 9
Arregui I., 2018, Adv. Space Res., 61, 655
Arregui I., 2021, ApJ, 915, L25
Arregui I., 2022, Front. Astron. Space Sci., 9, 826947
Aschwanden M. J., Schrijver C. J., 2011, ApJ, 736, 102
Aschwanden M. J., Fletcher L., Schrijver C. J., Alexander D., 1999, ApJ, 520, 880
Aschwanden M. J., De Pontieu B., Schrijver C. J., Title A. M., 2002, Sol. Phys., 206, 99
Brady C. S., Verwichte E., Arber T. D., 2006, A&A, 449, 389
Conde C. S. M., Jain R., Jatenco-Pereira V., 2022, ApJ, 931, 151
Dai J., Zhang Q. M., Su Y. N., Ji H. S., 2021, A&A, 646, A12
De Moortel I., Brady C. S., 2007, ApJ, 664, 1210
De Moortel I., Hood A. W., Ireland J., 2002, A&A, 381, 311
Goddard C. R., Nakariakov V. M., 2016, A&A, 590, L5
Goddard C. R., Nisticò G., Nakariakov V. M., Zimovets I. V., 2016, A&A, 585, A137
Goossens M., Hollweg J. V., Sakurai T., 1992, Sol. Phys., 138, 233
Goossens M., Andries J., Arregui I., 2006, Philos. Trans. R. Soc. A, 364, 433
Hindman B. W., Jain R., 2014, ApJ, 784, 103
Klimchuk J. A., DeForest C. E., 2020, ApJ, 900, 167
Lemen J. R. et al., 2012, Sol. Phys., 275, 17
Magyar N., Van Doorsselaere T., 2016, A&A, 595, A81
Mandal S., Tian H., Peter H., 2021, A&A, 652, L3
Nakariakov V. M., Kolotkov D. Y., 2020, ARA&A, 58, 441
Nakariakov V. M., Ofman L., 2001, A&A, 372, L53
Nakariakov V. M., Yelagandula N. V., 2023, Universe, 9, 95
Nakariakov V. M., Ofman L., Deluca E. E., Roberts B., Davila J. M., 1999, Science, 285, 862
Nakariakov V. M. et al., 2021, Space Sci. Rev., 217, 73
Nechaeva A., Zimovets I. V., Nakariakov V. M., Goddard C. R., 2019, ApJS, 241, 31
Nisticò G., Nakariakov V. M., Verwichte E., 2013, A&A, 552, A57
Ofman L., Aschwanden M. J., 2002, ApJ, 576, L153
Pascoe D. J., Hood A. W., De Moortel I., Wright A. N., 2013, A&A, 551, A40
Pascoe D. J., Goddard C. R., Nisticò G., Anfinogentov S., Nakariakov V. M., 2016a, A&A, 585, L6
Pascoe D. J., Goddard C. R., Nisticò G., Anfinogentov S., Nakariakov V. M., 2016b, A&A, 589, A136
Pascoe D. J., Anfinogentov S., Nisticò G., Goddard C. R., Nakariakov V. M., 2017, A&A, 600, A78
Pascoe D. J., Goddard C. R., Van Doorsselaere T., 2020, Front. Astron. Space Sci., 7, 61
Pesnell W. D., Thompson B. J., Chamberlin P. C., 2012, Sol. Phys., 275, 3
Ruderman M. S., Petrukhin N. S., 2022, Sol. Phys., 297, 116
Ruderman M. S., Roberts B., 2002, ApJ, 577, 475
Ruderman M. S., Verth G., Erdélyi R., 2008, ApJ, 686, 694
Selwa M., Ofman L., Solanki S. K., 2011, ApJ, 726, 42
Terradas J., Andries J., Goossens M., Arregui I., Oliver R., Ballester J. L., 2008, ApJ, 687, L115
Tian H., McIntosh S. W., Wang T., Ofman L., De Pontieu B., Innes D. E., Peter H., 2012, ApJ, 759, 144
Van Doorsselaere T. et al., 2020, Space Sci. Rev., 216, 140
Van Doorsselaere T., Goossens M., Magyar N., Ruderman M. S., Ismayilli R., 2021, ApJ, 910, 58
Verwichte E., Van Doorsselaere T., White R. S., Antolin P., 2013, A&A, 552, A138
Wang T., Ofman L., Davila J. M., Su Y., 2012, ApJ, 751, L27
Zhang Q. M., Chen J. L., Li S. T., Lu L., Li D., 2022, Sol. Phys., 297, 18
Zhong S., Nakariakov V. M., Kolotkov D. Y., Verbeeck C., Berghmans D., 2022, MNRAS, 516, 5989
Zimovets I. V., Nakariakov V. M., 2015, A&A, 577, A4

APPENDIX A: MODEL COMPARISON USING SOBAT

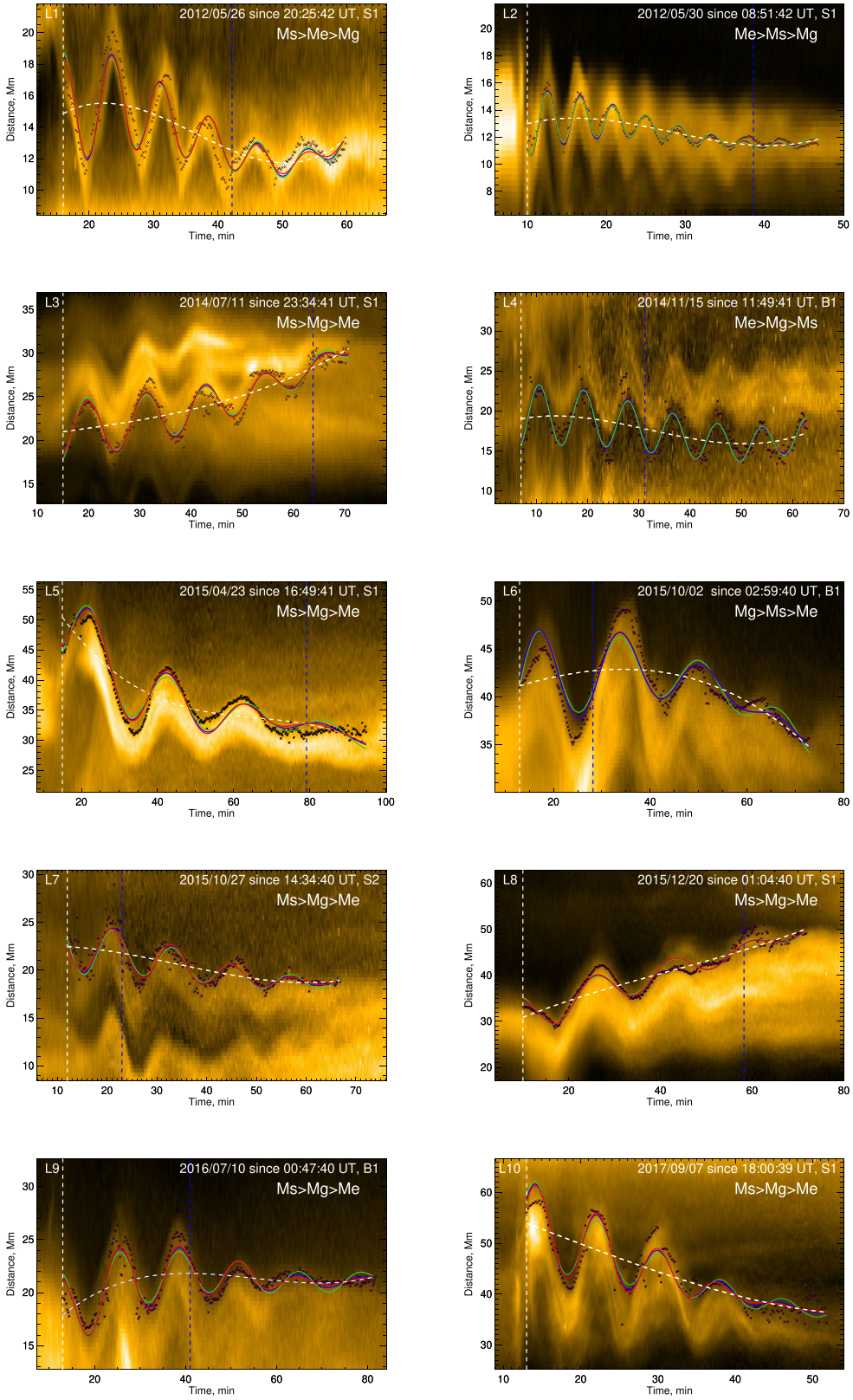

Figure A1. Decaying kink oscillations of 10 coronal loops (L1–L10) and their SOBAT analysis results. The black dots are the oscillatory signals. The green, red, and blue curves represent the MCMC fitting results of the exponential, superexponential, and Gaussian–exponential models, respectively. The white dashed curves in each panel represent their background trend. The white and blue vertical dashed lines indicate the start time t_0 of each signal and switch time t_s in the Gaussian–exponential model, respectively.

This paper has been typeset from a TEX/LATEX file prepared by the author.